PCCP

Accepted Manuscript

ROYAL SOCIETY OF CHEMISTRY

www.rsc.org/pccp

Journal Name

RSCPublishing

ARTICLE

Structural, elastic and vibrational properties of nanocrystalline lutetium gallium garnet under high pressure

Cite this: DOI: 10.1039/x0xx00000x

Received 00th January 2012,
Accepted 00th January 2012

DOI: 10.1039/x0xx00000x

www.rsc.org/

V. Monteseguro[a], P. Rodríguez-Hernández[a,b], H. Ortiz[c,d,e], V. Venkatramu[f], F. J. Manjón[c], C. K. Jayasankar[g], V. Lavín[a,h], and A. Muñoz[a,b,*]

An ab initio study of the structural, elastic and vibrational properties of the lutetium gallium garnet ($Lu_3Ga_5O_{12}$) under pressure has been performed in the framework of the density functional theory, up to 95 GPa. Pressure dependence of the elastic constants and the mechanical stability are analyzed, showing that the garnet structure is mechanically unstable above 87 GPa. Lattice-dynamics calculations in bulk at different pressures have been performed and contrasted with Raman scattering measurements of the nanocrystalline Tm^{3+}-doped LuGG up to 60 GPa. The theoretical frequencies and pressure coefficients of the Raman active modes for bulk LuGG are in good agreement with the experimental data measured in the nano-crystals. The contributions of the different atoms to the vibrational modes have been analyzed on the basis of the calculated total and partial phonon density of states. The vibrational modes have been discussed in relation to the internal and external modes of the GaO_4 tetrahedron and the GaO_6 octahedron. The calculated infrared modes and their pressure dependence are also reported. Our results show that with this nano-garnet size the sample has essentially bulk properties.

Introduction

The combination of the great luminescence properties of rare earth (RE^{3+})-doped garnets and their hardness, high optical transparency, high thermal conductivity, and mechanical and chemical stability makes them extremely useful as laser materials and as optical pressure and temperature sensors for extreme condition experiments, as alternative to ruby.[1] Moreover, large efforts have been spent to investigate the luminescence properties of RE^{3+}-doped nano-structured garnets,[2] especially in the development of lasers and phosphors in lightning applications, sensing and imaging in biomedicine, and as an alternative to quantum dots in photonic and optoelectronic devices for engineering.[3] Whereas the chemistry and properties of the garnet bulk crystals are more or less well known, the study of RE^{3+}-doped nano-garnets open the possibility to establish meaningful comparisons between the properties of the nano-sized and the bulk garnets.[4]

Due to the numerous practical applications of garnets and nano-garnets, there is a great interest in understanding their properties. In particular, the study of their elastics properties and mechanical stability under pressure is an interesting subject that can provide important information concerning the study of their structural transformations via the stability criteria. Besides, since phonons play an important role in the electrical, thermal and optical properties of materials it is essential to study its lattice dynamic to go deeper into the physics of these materials. The application of pressure allows the variation of the interatomic distances and bonds, and to obtain the structure dependence of the f-electron states in RE^{3+} ions.[5] The knowledge of the evolution of the elastic properties and the lattice dynamics of garnets under pressure could allow understanding possible changes occurring in the solid-state properties of the garnet and how they would affect the environment and, hence, the luminescence properties of RE^{3+} at high pressures. Moreover, the study of the garnet structure at high pressures is interesting for earth science, since garnet minerals are considered one of the major components of the deep interior of the Earth.[6]

There are several studies about luminescence properties of the RE^{3+} -doped $Lu_3Ga_5O_{12}$ (LuGG) bulk and nano-structured garnets due to their interesting properties and potential practical applications. [7, 8] However and to our knowledge, neither experimental nor theoretical studies of their elastic and lattice dynamics properties both at ambient conditions and at high pressures have been carried out so far. In the literature, few papers report the vibrational properties of garnets, most of them

devoted to the rare earth aluminum garnets ($RE_3Al_5O_{12}$) as $Lu_3Al_5O_{12}$ (LuAG), which is isostructural to LuGG.[9, 10] Recently, the pressure evolution of the vibrational properties of $Y_3Ga_5O_{12}$ (YGG), which is also isostructural to LuGG, has been studied both through experiments and first principles simulations;[11] furthermore, the elastic properties of this garnet under pressure have been analyzed by means of *ab initio* methods.[12] Now we are interested to study similar effects in our system, to evaluate the modifications related with the possible effect of the "chemical pressure" related with size effects when changing Y by Lu atom.

It should be noted that the theoretical studies under pressure of garnets are limited because of its high computational complexity.[13, 14] In spite of the fact that the use of *ab initio* density functional theory (DFT) calculations for the study of materials under extreme conditions is a very well established technique in the field of high pressure Semiconductor Physics,[15] most of the theoretical studies of some of the best-known garnets, like $Y_3Al_5O_{12,}$ have been performed by means of atomistic approach involving semi-empirical interatomic potentials with the rigid ion model (RIM)[14] and by first-principles density functional theory (DFT) calculations only for the ground-state.[16] In this work, we report an extensive study of the structural, elastic and vibrational properties of LuGG garnet at ambient conditions and under hydrostatic pressure using state of the art first principles total-energy calculations. Pressure dependence of the elastic constants and the mechanical stability of the garnet structure are analyzed to predict the phase transition at ultrahigh pressure. Raman scattering measurements in nanocrystalline Tm^{3+}-doped LuGG up to 60 GPa are presented and compared with the results of lattice dynamics *ab initio* calculations for bulk garnet up to 95 GPa.

Ab initio calculations

Ab initio total-energy calculations have been performed within the framework of density functional theory.[17] The VASP package was used to carry out calculations with the pseudopotential method and the projector augmented wave scheme (PAW).[18] Ultra-soft pseudopotentials, which replace the core electrons and make smoothed pseudovalence wave functions, were employed. For lutetium, 4 valence electrons were used ($4f^{14}5d^16s^2$), whereas 13 valence electrons ($3d^{10}4s^24p^1$) for gallium and 6 valence electrons ($2s^22p^4$) were used for oxygen. Highly converged results were achieved by extending the set of plane waves up to a kinetic energy cutoff of 520 eV. The exchange-correlation energy was taken in the generalized gradient approximation (GGA) with the PBEsol prescription.[19] A dense Monkhorst-Pack grid of k-special points was used to perform integrations along the Brillouin zone (BZ) in order to obtain very well converged energies and forces. At each selected volume, the structure was fully relaxed to its equilibrium configuration through the calculation of the forces on atoms and the stress tensor. It should be noted that, within the DFT formalism, the theoretical pressure, P(V), can be determined at the same time as the total energy, E(V), but independently since P (like other derivatives of the energy) can be obtained from the calculated stress[15]. In the relaxed configurations, the forces on the atoms are less than 0.006 eV/Å and the deviation of the stress tensor from a diagonal hydrostatic form is less than 0.1 GPa. The calculated total energies versus volumes are fitted using a standard equation of state (EOS) to determine the bulk modulus and its pressure derivatives.

The elastic constants are obtained computing the macroscopic stress for a small strain with the use of the stress theorem.[20] Alternatively, they can be also calculated using density functional perturbation theory (DFPT).[21] The ground state and fully relaxed structures at different pressures were strained in different directions according to their symmetry. The total-energy variations were evaluated according to a Taylor expansion[22] for the total energy with respect to the applied strain. Due to this fact it is important to check that the strain used in the calculations guarantees the harmonic behavior. This method allows to obtain the C_{ij} elastic constants in the Voigt notation; the number of independent elastic constants is reduced completely by crystalline symmetry.[23] The elastic constants enable the study of the mechanical properties and the mechanical stability of materials in the region where the strain-stress relations are still linear.

Lattice-dynamics calculations were performed at the zone center (Γ point) of the BZ. Highly converged results on forces are required for the calculation of the dynamical matrix using the direct force constant approach.[24]The construction of the dynamical matrix at the Γ point of the BZ involves separate calculations of the forces in which a fixed displacement from the equilibrium configuration of the atoms within the primitive cell is considered. The number of such independent displacements in the analyzed structure is reduced due to the crystal symmetry. Diagonalization of the dynamical matrix provides the frequencies of the normal modes. Moreover, these calculations allow identifying the symmetry and eigenvectors of the vibrational modes in each structure at the Γ point.

Experimental details

Nanocrystalline lutetium gallium garnet doped with thulium ions $Lu_{3(1-x)}Tm_{3x}Ga_5O_{12}$ (x=0.01) was synthesized by the citrate sol-gel method in air atmosphere.[25] Stoichiometric molar ratio of high-purity $Ga(NO_3)_3{\cdot}9H_2O$, $Lu(NO_3)_3{\cdot}4H_2O$ and $Tm(NO_3)_3{\cdot}5H_2O$ materials were dissolved in 25 ml of 1 M HNO_3 under stirring at 353 K for 3 h. Then citric acid, with a molar ratio of metal ions to citric acid of 1:2, was added to the solution, which was stirred for 2 h more and finally dried at 363 K for 36 h. This process created a gel that was fired at 773 K for 4 h to remove the residual nitrates and organic compounds and the subsequently obtained powder sample was finally calcined at 1173 K for 16 h. The structure of the LuGG nano-garnet at ambient pressure was checked by X-ray diffraction using the $CuK_{\alpha 1}$ (1.5406 Å) radiation in the range of 2θ= 10º–80º, with a step size of 0.020º (PANalytical X'Pert Pro). The average crystallite size was estimated to be around 60 nm for the LuGG nano-garnet under study from the full width at half maximum (FWHM) of the diffraction peak at 32.71º using the Scherrer's equation along with the structure of the unit cell, and it was confirmed with HRTEM micrographs.[26]

The prepared nano-powder sample of Tm^{3+}-doped LuGG, along with a 2-μm-diameter ruby ball, was loaded in a pre-indented tungsten gasket with a 150-μm-diameter hole inside a diamond-anvil cell. A 16:3:1 methanol-ethanol-water mixture was used as pressure-transmitting medium and the pressure was determined by monitoring the shift in ruby fluorescence lines.[27] The methanol-ethanol-water mixture is a hydrostatic medium up to 10.5 GPa; after this pressure, it behaves quasi-hydrostatically.[28, 29] High-pressure Raman scattering measurements were performed in backscattering geometry using a 632.8 nm HeNe laser and a microspectrometer (LabRAM HR UV, Horiba-Jobin Yvon) in combination with a

thermoelectrically-cooled multichannel CCD detector (Synapse, Horiba-Jobin Yvon) with spectral resolution better than 2 cm^{-1}. Experimental frequencies of the Raman modes were obtained by fitting peaks with a Voigt profile (lorentzian convoluted with a gaussian) after proper calibration and background subtraction of the experimental spectra. The gaussian linewidth was fixed to the experimental setup resolution in order to get the three variables of the lorentzian profile for each peak.

Results and discussion

3.1 Crystal structure and bulk properties

Oxide garnets have the general formula $A_3B_2C_3O_{12}$. For the lutetium gallium garnet, $Lu_3Ga_5O_{12}$, *A* atoms correspond to lutetium (Lu) while *B* and *C* atoms correspond to gallium (Ga). LuGG crystallizes in the body-centered cubic (bcc) structure (space group Ia-3d, No. 230, Z=8) and has 160 atoms in the conventional unit cell (80 in the primitive cell). Two of the five Ga atoms in the formula unit occupy octahedral sites of S_6 symmetry (Wyckoff position 16a) while the other three atoms occupy tetrahedral sites of S_4 symmetry (Wyckoff position 24d). The three Lu atoms (or substitutional Tm^{3+} atoms) are in dodecahedral sites of D_2 symmetry (Wyckoff position 24c), and the twelve O anions are in Wyckoff positions 96h that are characterized by three structural parameters (x, y, z).[30] The garnet structure can be viewed as a network of LuO_8 dodecahedra, GaO_6 octahedra and GaO_4 tetrahedra interconnected with shared O atoms at the corners (Figure 1).

Energy-volume data have been analyzed using a third-order Birch-Murnaghan equation of state (EOS).[31] Table I summarizes the theoretical structural parameters of LuGG and the atomic positions at ambient pressure. The theoretical lattice constant of the LuGG bulk crystal, 12.17 Å, compares very well with the experimental data for the bulk LuGG, 12.19 Å[30] and also with the unit cell parameter of the Tm^{3+}-doped LuGG nano-garnet obtained from X-ray diffraction, 12.20 Å. This result suggests that, at least from the structural point of view, our nano-garnets with 60-nm-grain size should behave as bulk garnet material. We will show along this paper that the same applies for the vibrational properties.

The bulk modulus, B_0, and its pressure derivative, B_0', are summarized in Table I. It must be noted that the bulk modulus, 177.8 GPa, is similar to those of most silicate garnets (between 150 and 180 GPa).[32] LuGG garnet has a smaller bulk modulus, and larger volume, V_0=905.3 $Å^3$, than aluminum garnets such as $Lu_3Al_5O_{12}$ with bulk modulus B_0 = 192.4 GPa and volume V_0 = 831.7 $Å^3$, and $Y_3Al_5O_{12}$ with bulk modulus B_0 = 183.9 GPa and volume V_0 = 867.9 $Å^3$.[33] On the other hand, the LuGG has a larger bulk modulus and smaller volume than other gallium garnets, like $Y_3Ga_5O_{12}$ with B_0 = 170.7 GPa and volume V_0 = 925.5 $Å^3$, [12] which can be ascribed to the slightly smaller ionic radius of the Lu (Z=71) atom, compared to the Y (Z=39) one, due to the lanthanide contraction effect.

To illustrate the structural changes of LuGG at different pressures, Figure 2 shows the evolution of the interatomic distances as function of pressure. The main cation-anion bond distances at selected pressures are summarized in Table II. At ambient pressure, LuO_8 dodecahedra are slightly distorted with Lu-O distances ranging from 2.29 to 2.36 Å while the Ga_{oct}-O and Ga_{tet}-O distances are 1.98 Å and 1.84 Å for GaO_6 and GaO_4, respectively. Comparing these cation-anions distances with those in the $Y_3Ga_5O_{12}$ (YGG), a garnet belonging to the same family of gallium garnets, the mayor difference is found, in the slightly longer Y-O distances of the dodecahedra, ranging from 2.34 to 2.42 Å in YGG. However, the Ga_{oct}-O and Ga_{tet}-O distances, 1.99 Å and 1.84 Å, respectively, are the same in both structures.

As observed all the distances decrease with increasing pressure. Although our calculations show that whereas the Ga_{tet}-O and Ga_{oct}-O distances decrease at similar rates of $-2.1\cdot10^{-3}$ Å/GPa and $-2.6\cdot10^{-3}$ Å/GPa respectively, not all Lu-O distances change at the same rate. The smallest distance, labeled as Lu-O1, changes at a rate of $-2\cdot10^{-3}$ Å/GPa, while the largest Lu-O2 distance varies faster, about $-5.6\cdot10^{-3}$ Å/GPa. Noteworthy, both Lu-O distances becomes equal around 23.29 GPa with a Lu-O distance of 2.327 Å. This effect is very common among garnets; e.g. in the GGG, the Gd-O distances become equal between 8 and 11 GPa.[34] The similar decrease of the Lu-Ga_{tet} and Lu-Ga_{oct} distances (with rate of $-5\cdot10^{-3}$ Å/GPa) on increasing pressure indicates that the influence between dodecahedra and tetrahedra or octahedra is similar in all the pressure range up to 90 GPa.

3.2 Elastic properties

Cubic crystals, as LuGG, are characterized by an elastic constant tensor with only three independent elastic constants, C_{11}, C_{12}, and C_{44}. The computed elastic constants at zero pressure are show in Table III. A lattice is mechanically stable at zero pressure only if the Born stability criteria are fulfilled.[35] In the case of cubic systems these criteria are:

$$C_{11} + 2\,C_{12} > 0,\ C_{11} - C_{12} > 0 \text{ and } C_{44} > 0 \quad (1)$$

As expected, the calculated set of elastic constants satisfies the above criteria, confirming that cubic LuGG is mechanically stable at ambient pressure.

When a non-zero uniform stress is applied to the crystal, the above criteria to describe the stability limits of the crystal at finite strain are not adequate and the Born stability criteria must be modified. In this case, the elastic stiffness coefficients are defined as

$$c_{ijkl} = C_{ijkl} + 1/2\,[\,\delta_{ik}\sigma_{jl} + \delta_{jk}\sigma_{il} + \delta_{il}\sigma_{jk} + \delta_{jl}\sigma_{ik} - 2\,\delta_{kl}\sigma_{ij}] \quad (2)$$

where the C_{ijkl} are the elastic constants evaluated at the current stressed state, σ_{ij} correspond to the external stresses, and δ_{jl} is the Kronecker delta. In the special case of hydrostatic pressure applied to a cubic crystal, $\sigma_{11} = \sigma_{22} = \sigma_{33}$, and the elastic stiffness coefficients are: $c_{11} = C_{11} - P$, $c_{12} = C_{12} + P$, and $c_{44} = C_{44} - P$. The new conditions for the elastic stability, known as the "generalized Born stability criteria" are obtained by replacing in Eq. (1) the elastic constants C_{ij} by the stiffness coefficients c_{ij}.[36] Therefore, a cubic crystal, as LuGG, is mechanically stable under hydrostatic pressure when the generalized Born stability criteria:

$$M_1 = (C_{11} + 2\,C_{12} + P) > 0,\ M_2 = (C_{11} - C_{12} - 2\,P) > 0 \text{ and } M_3 = C_{44} - P > 0 \quad (3)$$

are simultaneously satisfied.

The evolution of the calculated C_{ij} up to 90 GPa is plotted in Figure 3. It can be seen that the C_{11} and C_{12} elastic constants increase as pressure increase, while the C_{44} elastic constant remains almost constant with a value of approximately 100 GPa along the whole range of pressure investigated (0-90 GPa). C_{11} is higher than C_{44}, indicating that in this material the resistance to a shear deformation is weaker than the resistance to a compression.

M_1, M_2, and M_3 versus pressure are plotted in Figure 4. It is found that the $M_2 > 0$ stability criterion is violated at 87 GPa and the criterion $M_3 > 0$ is also violated but at a higher pressure,

suggesting that LuGG becomes mechanically unstable above 87 GPa. This pressure is an upper bound which indicates either an amorphization or a phase transition of the LuGG at this pressure. The softening of the tetragonal shear modulus M_2 and the shear modulus M_3 suggest shear instability of the cubic structure. In some cubic binary compound, this softening can be related with some phase transition mechanism.[37] For gallium oxide garnets, Hua *et al*.[38] have reported high pressure and high temperature studies of the Cr^{3+} and Nd^{3+}-doped gadolinium gallium garnet $Gd_3Ga_5O_{12}$ (GGG) and the Cr^{3+}, Nd^{3+}-doped gadolinium scandium gallium garnet $Gd_3Sc_2Ga_3O_{12}$ (GSGG).[38] The experimental results show that an amorphous phase appears over 54 GPa and 84 GPa in GSGG and GGG, respectively. These results are similar to those of aluminium garnets, like YAG, which is found to retain its crystalline cubic phase up to 101 ± 4 GPa.[38] *Ab initio* studies report the mechanical instability of yttrium gallium garnet (YGG) above 84 GPa.[12] Therefore, our results for LuGG are in good agreement with the reported experimental data for other gallium garnets and suggest that LuGG will become amorphous at around 87 GPa.

The elastic stiffness enable to obtain also the major elastic properties of a material described by the bulk modulus (B), the Zener anisotropy ratio (A), the isotropic shear modulus (G), the Young modulus (E), the Poisson's ratio (ν), and B/G relation given by:

$$B = \frac{c_{11} + 2\,c_{12}}{3}$$
$$A = \frac{2\,c_{44}}{c_{11} - c_{12}}$$
$$G = \frac{1}{2}\left[\frac{c_{11}-c_{12}+3\,c_{44}}{5} + \frac{5\,c_{44}\,(c_{11}-c_{12})}{4\,c_{44}+3\,(c_{11}-c_{12})}\right] \quad (4)$$
$$E = \frac{9\,B\,G}{(3B)+G}$$
$$\nu = \frac{E-2G}{2G}$$

The values of these parameters for LuGG at zero pressure are summarized in Table III. The bulk modulus, i.e. the inverse of the compressibility, is an important parameter related with the resistance of the material to a uniform hydrostatic pressure. It is interesting to mention that the bulk modulus at zero pressure, $B_0 = (C_{11} + 2\,C_{12})/3$, computed from the values of the elastic constants (173.9 GPa) is in good agreement with the one obtained from the total-energy calculations using the EOS (Table I). The coincidence of both results indicates the quality and consistency of our calculations. The Zener anisotropy ratio A is 1.2, nearly 1, thus suggesting that LuGG has an isotropic crystalline structure. According to the Pugh criterion,[39] a value of B/G above 1.75 indicates a tendency to behave as a ductile material. In our case B/G is 1.9 which indicates that LuGG is a ductile material. The Young´s modulus and the Poisson's ratio are two important parameters for engineering and technological applications. The first one, 235.2 GPa, provides a measure of the stiffness while the second one is 0.28, close to 0.25 and points out that LuGG, at zero pressure, is a material with predominant central internal forces; i.e the high coordination of the atoms induces a quasi-spherical symmetry in the system causing the central forces to dominate the mechanical properties.

To conclude this section, we comment the pressure dependence of the elastic moduli (B, G, and E) reported in Figure 5. The bulk modulus, B, increases while the shear moduli, G and the Young modulus, E, decrease with the pressure. The bulk modulus equals the Young modulus, E, at 15.7 GPa hence LuGG offers the same resistance to an uniform than to a one-directional compression at this pressure. The ratio of bulk to shear moduli, B/G, increases (26.7 at 80 GPa) so the garnet becomes more ductile with increasing pressure. The Poissons´s ratio, ν, slightly increases to 0.48 before the crystal becomes unstable. The Zener anisotropy ratio, A, decreases up to negative values above 87 GPa. This result indicates that the isotropy of the material disappears as the pressure increases.

3.3 Lattice dynamics

In this section we will analyze the theoretical and experimental results of the lattice dynamics of LuGG first at ambient pressure and then at high pressures.

3.3.1 At ambient pressure

According to group theoretical considerations, the Ia-3d structure of LuGG has 97 vibrational modes that can be classified at the BZ center as 25 Raman-active modes (Γ_R), 17 infrared-active modes (Γ_{IR}), 55 optically-inactive (silent) modes (Γ_S), and 1 acoustic (T_{1u}) mode.

$$\Gamma_R = 3A_{1g} + 8E_g + 14T_{2g}$$
$$\Gamma_{IR} = 17T_{1u}$$
$$\Gamma_S = 16T_{2u} + 14T_{1g} + 5A_{2u} + 5A_{2g} + 10E_u + 5A_{1u}$$

where the A modes are non-degenerated, and E and T (also noted F in the literature) modes are doubly and triply degenerated, respectively.

Only 17 out of the 25 Raman-active modes theoretically predicted have been experimentally measured. This is probably due to an accidental degeneracy of several modes or because some modes are too weak to be observed. The unpolarized Raman spectrum of Tm^{3+}-doped LuGG nano-crystals at ambient conditions can be observed in Figure 6. For comparison the vertical marks at the bottom of the figure represent the theoretical frequencies of the Raman-active modes predicted at ambient conditions for bulk LuGG. All experimental and theoretical Raman-active modes frequencies at room pressure are summarized in Table IV. The similarity of the Raman frequencies for the Tm^{+3} –doped LuGG nanogarnet with those calculated for pure LuGG evidence that 1% Tm^{+3} doping does not have any effect in the vibrational properties of LuGG and that 60 nm size nanocrystalline LuGG garnet shows the same vibrational properties than LuGG bulk garnet.

The Raman spectrum of LuGG can be divided into two regions: the low frequency region (80 - 550 cm^{-1}) and the high frequency region (550 - 730 cm^{-1}), as in the case of YGG. [11] This division contrasts with that of the Raman spectrum of YAG, which has three regions.[40] This can be understood if one considers that gallium garnets have a larger unit cell volume than that of aluminum garnets and that gallium is heavier than aluminum. Consequently, there is a redshift in the high-frequency modes of gallium garnets compared to the aluminum ones, which results in an overlapping of the high and intermediate regions in LuGG. Moreover, the heavy mass of Lu and RE atoms must be taken into account, since the values of the frequencies decrease as the mass of the *A* atoms of the $A_3B_2C_3O_{12}$ garnet increases.

The symmetries of the observed modes (see Figure 6) are assigned on the basis of our theoretical calculations and on the comparison with previous works of lattice dynamics in

garnets.[9, 41] The fourth peak of lowest frequency in Figure 6, observed around 200 cm^{-1}, corresponds to a Raman second order peak and; for this reason, no assignation of symmetry has been given. There is a quite good agreement between the experimental modes measured in the Tm^{+3} doped nanogarnet and the theoretical vibrational frequencies of bulk LuGG summarized in Table IV. Only slight shifts in some frequencies have been found between experimental and theoretical Raman-mode frequencies, which can be attributed to the GGA approximation which tends to underestimate the vibrational frequencies.

The Raman spectra of garnets have been usually interpreted assuming that the different Raman modes could be attributed to the vibrational modes of the tetrahedral (GaO_4), octahedral (GaO_6), and dodecahedral (LuO_8) units. However, it must be considered that the vibrations of the different polyhedra are strongly coupled to each other, so the attribution of each Raman mode to a single unit is not straightforward. Therefore, to understand the contribution of each polyhedral unit to every Raman mode, we have calculated the total and partial (or projected onto each atom) phonon density of states shown in Figure 7. In this figure, the dynamical contribution of each atom can be observed. Lu atoms contribute in the low-frequency region between 80 and 270 cm^{-1} with especial intensity in the region between 80 and 150 cm^{-1}.

Ga atoms with octahedral coordination (Ga_{oct}) predominantly contribute in the low-frequency region between 80 and 400 cm^{-1} with a maximum around 420 cm^{-1} and a small contribution about 500 cm^{-1}. Ga atoms with tetrahedral coordination (Ga_{tet}) have the greatest contribution in the low-frequency region (between 80 and 400 cm^{-1}), but also contribute in the high-frequency region (between 550 and 730 cm^{-1}). Finally, O atoms contribute in both the low- and high-frequency regions.

Once known the contributions of the individual atoms, we can now discuss the contributions of the different polyhedra to each vibrational mode. The phonon modes of a garnet crystal with general formula $A_3B_2C_3O_{12}$ (*A*, *B* and *C* being cations), can be described as a combination of the molecular modes of the CO_4 and BO_6 polyhedra,[41] the GaO_4 and the GaO_6 tetrahedra in our case. This outline has been used to describe the phonon modes of silicon[42], aluminium[9] and gallium garnets[11]. Due to the structural similarity of aluminum and gallium garnets, the internal Raman modes of LuGG could be assigned in a similar way as they have been, usually, assigned in YAG,[9, 41] and, recently, in YGG[11]. The most intense Raman modes of LuGG correspond to the three A_{1g} modes (see Fig. 6). These three modes are directly connected with the free GaO_4 and GaO_6 internal vibrations. The higher frequency A_{1g} mode corresponds to the symmetric stretching mode of tetrahedra and octahedra. The intermediate A_{1g} mode might be related with the bending mode of tetrahedra and octahedra and, finally, the lower frequency A_{1g} mode can be assigned to the rotational mode of octahedra and a small contribution of a rotational mode of the tetrahedra.

In the low-frequency region, translational movements of GaO_4 and LuO_8 units can be observed; however, the GaO_6 units do not have associated any translational movement in the garnet structure. The first T_{2g} mode at 95 cm^{-1} and the first E_g mode at 105 cm^{-1} correspond to translational movements of the polyhedra GaO_4 and LuO_8. In particular, in the E_g mode at 105 cm^{-1}, the translation of the dodecahedra is greater than those of the tetrahedra. The following four T_{2g} modes at 138, 161, 176 and 231 cm^{-1} and the E_g mode at 249 cm^{-1} are mainly related to translational movements of the GaO_4 tetrahedra. Apparently, in these modes, there is no translational movement of the LuO_8 dodecahedra as a unit, although we can observe a translational movement of the Lu cations. The T_{2g} modes with frequencies of 397 cm^{-1} might be related with the rotational mode of GaO_4 tetrahedra and GaO_6 octahedra. The E_g mode at 477 cm^{-1} and the two T_{2g} modes with frequencies 490 and 511 cm^{-1} are assigned to symmetric bending modes of the GaO_4 and GaO_6 units. As for the other calculated modes, a complex vibrational pattern appears and it is not easy to distinguish the individual vibration of each polyhedra. It can only be said that the high-frequency region of the Raman spectrum corresponds to the vibrational modes of the oxygen atoms in GaO_4 and GaO_6 polyhedra.

The first theoretical mode, which has not been measured experimentally, has a frequency of 95 cm^{-1}. This result is not common between garnets. Usually the lowest frequency active mode is above 100 cm^{-1}. The unusually low frequency modes in LuGG are probably due to the fact that the Lu has a much greater mass than other *A* atoms in the garnets commonly studied. Therefore, we consider that the large mass of Lu atoms in the garnet structure has a strong influence on the complex vibrational pattern of LuGG, which is due to the dense structure of these compounds and the strong atomic interactions between the different polyhedra. These strong atomic interactions also account for the complexity of the vibrational pattern of garnets and the difficulty of explaining their vibrational modes in terms of the isolated polyhedral units.

3.3.2 High pressure

As previously mentioned, only 17 Raman-active modes are observed at 1 atm; however, the number of peaks observed changes at different pressures. The intensity of some of them increases at certain pressures, and they can be observed while others cannot be detected anymore. Selected experimental Raman spectra of nanocrystalline Tm^{3+}-doped LuGG at different pressures up to 60 GPa are shown in Figure 8. It should be mentioned that the degenerated peak near 350 cm^{-1}, which correspond to the A_{1g} and E_g modes at low pressure, can be individually identified above 6 GPa. In general, all phonon frequencies exhibit a monotonous increase with pressure up to 60 GPa due to the contraction of the interatomic distances in the unit-cell volume commented in *section IV*. A considerable broadening of Raman peaks with increasing pressure is observed, although no changes in the profile of the Raman spectrum are detected up to 60 GPa, the maximum pressure reached experimentally, thus suggesting that the bcc structure is stable up to this pressure.

The pressure dependences of the experimental and theoretical Raman-active mode frequencies up to 60 and 90 GPa, respectively, are shown in Figure 9. Experimental and theoretical frequencies and pressure coefficients are very similar at ambient conditions as well as at high pressures (see Table IV). This good agreement between the experimental and theoretical modes reflects, as already mentioned, that the introduction of RE^{3+} ions in the nano-garnet up to a concentration of 1% does not change the lattice dynamics of the material, and that the vibrational properties of our nano-garnets of size 60 nm are rather similar to those of the bulk garnet. This is a particularly successful result to be taken into account in different nano-technological applications.

It should be noted that all first-order pressure coefficients are positive and that the lowest-frequency Raman phonon mode, E_g (see Table IV) has a very small pressure coefficient, indicating

that these modes has very small volume dependence. The experimental and theoretical Grüneisen parameters, $\gamma = (B/\omega)(\partial\omega/\partial P)$, for the Raman modes, are summarized in Table IV. They have been estimated by using the theoretical value for the bulk modulus, B_0=177.8 GPa, obtained from the third-order Birch-Murnaghan EOS.[31] The theoretical (experimental) Grüneisen parameters have a greater variation in the region of low-frequency with γ ranging from 0.74 (0.66) to 1.78 (1.64), than in the high-frequency region, where it ranges from 0.93 (0.78) to 1.26 (1.39). Hence, there are larger differences in the restoring forces on the atoms of those polyhedra related to the lowest modes. The lowest E_g mode (mode assigned to the translation of LuO_8) has very small pressure coefficient and Grüneisen parameter at ambient pressure, indicating that the restoring force between LuO_8 units decreases as the pressure increases.

The larger contraction of distances related to lutetium (Lu-O2 distances) is not reflected in larger pressure coefficients for the modes related to Lu atoms between 100 and 270 cm^{-1}. In fact, the modes with the largest pressure coefficients are those with frequencies above 590 cm^{-1} that are related to Ga_{tet}, as it is suggested by Figure 6. These results would indicate that the decrease of the Lu-O2 bond force constant must be related to a charge transfer to some of the Ga-O bonds. This transfer should lead to a larger pressure coefficient of vibrational modes related to these Ga-O bonds. Therefore, on increasing pressure there must be an increase of the charge transfer mainly from Lu-O2 bonds to Ga-O bonds in GaO_4 tetrahedra. This is possible since the O2 atoms are shared between the dodecahedra and the tetrahedra.

Finally, as regards the infrared-active (IR) and silent vibrational modes, their theoretical frequency pressure dependence are plotted in Figures 10 and 11, respectively. Theoretical Grüneisen parameters of IR-active modes vary between 1.55 and 0.12. In fact, the second lowest frequency IR mode has the lowest Grüneisen parameter (see Table V). It is noteworthy that the two first T_{1u} infrared-active modes show a softening with increasing pressure, thus suggesting a possible pressure-induced instability.[21] This instability is clearly indicated by the evolution of the lowest frequency silent mode T_{2u} that becomes negative at 122 GPa. Therefore, this result is in agreement with our theoretical study of the mechanical stability of LuGG presented in section V, where it was shown that it becomes mechanically unstable above 87 GPa.

Figures

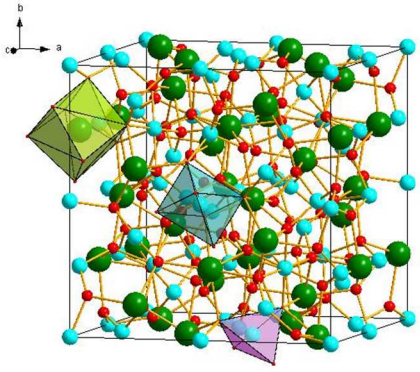

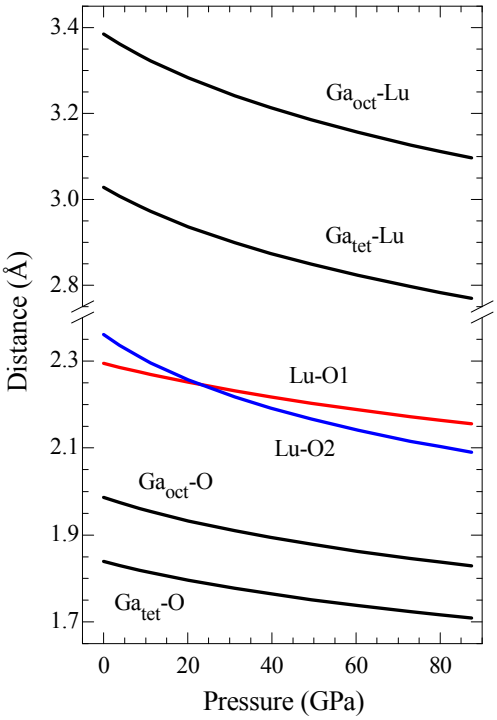

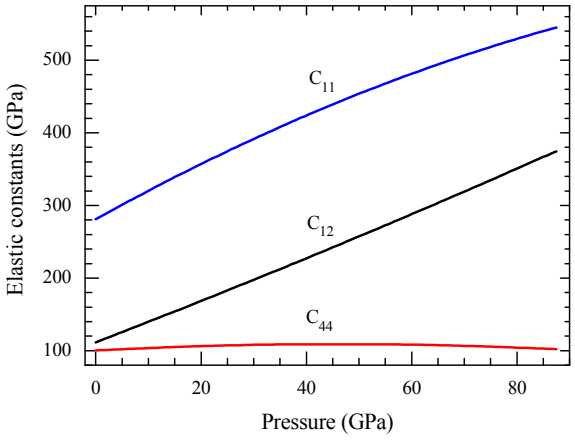

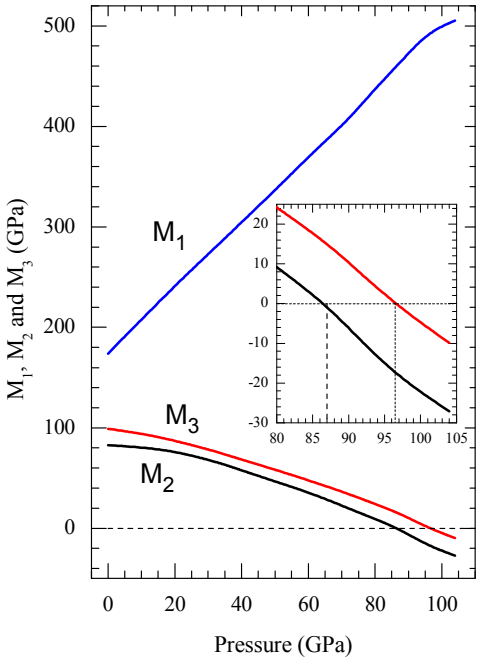

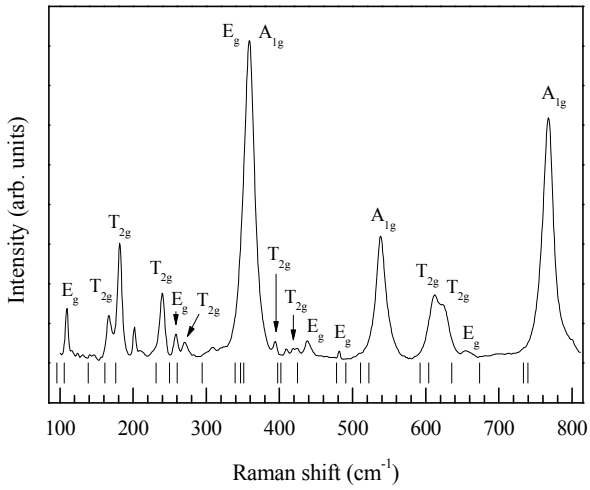

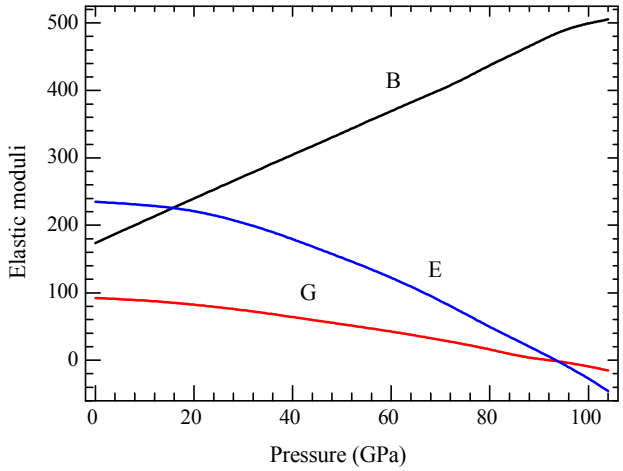

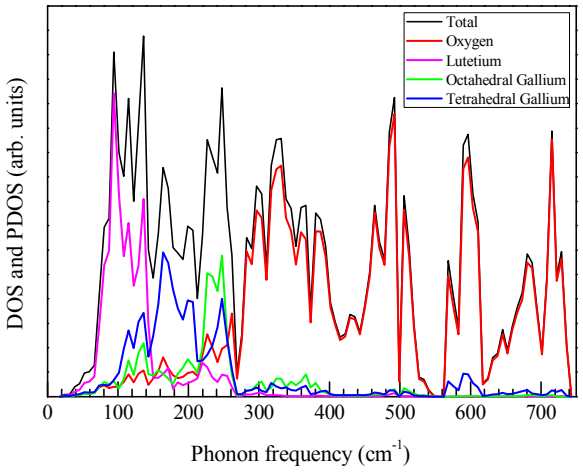

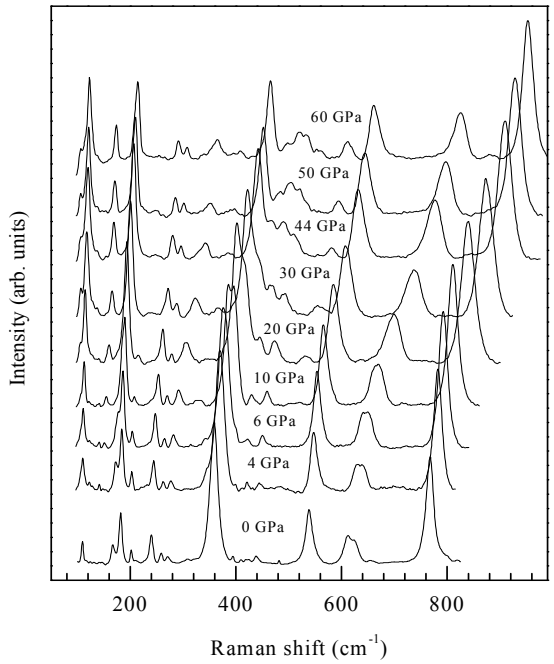

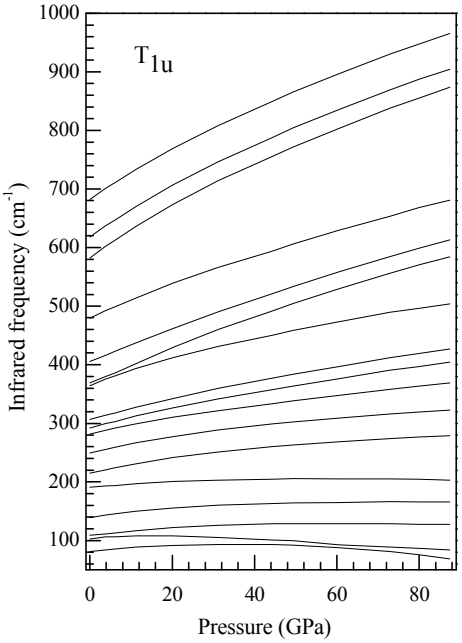

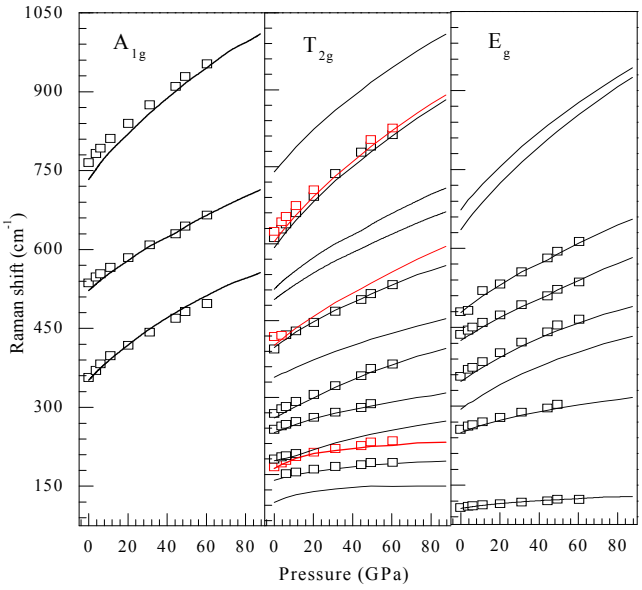

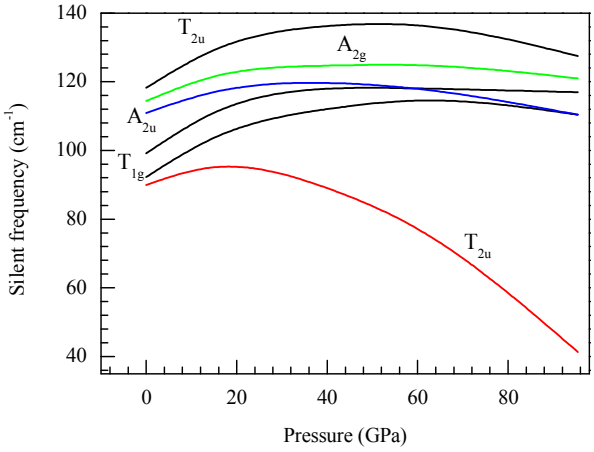

Tables

	Ab initio (this work)	Experimental[a]
a (Å)	12.17	12.19
V (Å^3)	901.2	905.3
Ga(16a)	0,0.5, 0	0,0.5, 0
Ga(24d)	0.75, 0.125, 0	0.75, 0.125, 0
Lu(24c)	0.25,0.875,0.5	0.25,0.875,0.5
O(96h)	0.099, 0.192, 0.276	0.099, 0.193, 0 .275
B_o(GPa)	177.8	-----
B’	4.7	-----

[a] Reference 30.

Cation-anion distances (Å)			
	0 GPa	31 GPa	87 GPa
Lu-O	(2.29 to 2.36)	(2.22 to 2.23)	(2.09 to 2.16)
Ga_{tet}-O	1.84	1.78	1.71
Ga_{oct}-O	1.98	1.91	1.83

C_{11} (GPa)	C_{12} (GPa)	C_{44} (GPa)	B (GPa)	G (GPa)	E (GPa)	ν	A	B/G
284.3	118.7	99.2	173.9	92.3	235.2	0.28	1.2	1.9

	Ab initio				Experimental			
Raman mode symmetry	ω_0 (cm^{-1})	$\partial\omega/\partial P$ (cm^{-1}/GPa)	$\partial^2\omega/\partial P^2$ (cm^{-1}/GPa^2) ($x10^{-3}$)	γ	ω_0 (cm^{-1})	$\partial\omega/\partial P$ (cm^{-1}/GPa)	$\partial^2\omega/\partial P^2$ (cm^{-1}/GPa^2) ($x10^{-3}$)	γ
T_{2g}	95.8	0.94	-7	1.78	-----	-----	-----	-----
E_g	105.9	0.43	-2	0.74	107.2	0.39	-2	0.66
T_{2g}	138.5	0.81	-5	1.06	151.1[b]	0.76	-5	-----
T_{2g}	161.4	1.21	-8	1.36	164.8	1.45	-11	1.59
T_{2g}	176.5	1.31	-4	1.34	179.6	1.24	-26	1.25
T_{2g}	231.2	1.30	-5	1.02	237.6	1.19	-5	0.9
T_{2g}	260.1	2.12	-6	1.48	268.5	1.77	-5	1.19
E_g	249.6	1.16	-5	0.84	256.1	1.17	-5	0.83
E_g	294.1	2.36	-9	1.45	-----	-----	-----	-----
T_{2g}	339.5	1.75	-5	0.93	-----	-----	-----	-----
A_{1g}	351.4	3.45	-13	1.78	356.4	3.22	-16	1.64
E_g	347.1	2.39	-9	1.25	356.4	2.31	-9	1.17
T_{2g}	397.5	2.48	-8	1.13	394.3	2.49	-9	1.14
T_{2g}	401.9	2.78	-7	1.25	418.5[c]	-----	-----	-----
E_g	425.0	2.12	-3	0.90	436.4	1.87	-4	0.78
E_g	477.9	2.53	-6	0.96	479.4	2.89	-12	1.09
T_{2g}	490.8	2.53	-7	0.93	-----	-----	-----	-----
T_{2g}	511.1	2.92	-8	1.04	-----	-----	-----	-----
A_{1g}	522.1	2.79	-7	0.97	536.4	2.35	-4	0.79
T_{2g}	592.2	4.40	-13	1.35	611.1	4.71	-22	1.39
T_{2g}	603.8	4.36	-13	1.31	623.5	4.51	-19	1.31
E_g	635.3	4.41	-13	1.26	652.4[c]	-----	-----	-----
E_g	673.4	4.10	-12	1.10	-----	-----	-----	-----
T_{2g}	739.6	4.12	-12	1.01	-----	-----	-----	-----
A_{1g}	733.3	4.37	-14	1.08	764.9	3.86	-13	0.91

[b] This mode appears above 6.11 GPa with the values indicated in the table

[c] These modes only appear at 0 GPa.

Infrared mode symmetry, T_{1u}			
ω (cm^{-1})	$\partial\omega/\partial P$ (cm^{-1}/GPa)	$\partial^2\omega/\partial P^2$ (cm^{-1}/GPa^2) ($x10^{-3}$)	γ
81.1	0.67	-9	1.49
102.3	0.07	-3	0.12
109.1	0.68	-5	1.13
138.9	0.76	-5	0.99
190.7	0.49	-4	0.47
214.6	1.29	-7	1.09
249.1	1.39	-7	1.01
281.6	1.32	-4	0.85
291.9	1.67	-4	1.04
306.5	1.82	-5	1.08
363.9	2.29	-8	1.14
369.0	3.15	-8	1.55
405.3	2.87	-6	1.28
479.4	2.89	-7	1.09
582.4	4.47	-14	1.39
617.8	4.39	-13	1.29
681.9	4.3	-13	1.14

Conclusions

An *ab initio* study of the structural, elastic and vibrational properties of $Lu_3Ga_5O_{12}$ (LuGG) under hydrostatic pressure was performed. The structural study of nanogarnets with size 60 nm as shown a similar lattice parameter than that of the bulk garnet and the bulk modulus of the nanogarnets is also similar to the theoretical one, thus suggesting that the nano-garnets behave as bulk from a structural point of view. The elastic properties of this material are analyzed at zero as well as at high pressure. The calculations show that the generalized stability conditions are no more fulfilled at 87 GPa and the garnet structure crystal becomes mechanically unstable. The theoretical results for the lattice dynamic of bulk LuGG under high pressure up to 90 GPa have been compared with experimental results from Raman scattering measurements in 60-nm size nanocrystalline Tm^{3+}-doped LuGG up to 60 GPa. A good agreement between theory and experiment has been found, which suggests that the introduction of a RE^{3+} in the nano-garnet, up to 1% concentration, does not change the lattice dynamics of the material and that the vibrational properties of our nano-garnets with size 60 nm are similar to those of the bulk garnet. It means that for the typical size of this nano-garnet one can use the structural, vibrational and optical properties of bulk material to correlate with changes in the optical properties of these materials when doped with optically active ions. Our study also shows that the effect of the "chemical pressure" has not large differences with similar results in YGG garnets.

We have analyzed the total and the partial phonon density of states in order to discuss the contribution of each atom to the different Raman vibrational modes. Lu atoms (or possible substituting RE^{3+}) and octahedrally-coordinated Ga atoms mainly contribute in the low-frequency region whereas the tetrahedrally-coordinated Ga and O atoms contribute in both low and high frequency regions. Moreover, the Raman phonon modes of LuGG crystal are associated to internal and external molecular modes of the different polyhedra. In the region, from 95 to 249 cm^{-1}, the translational modes of LuO_8 and GaO_4 dominate in the Raman spectrum while between 397 and 511 cm^{-1}, the rotational and bending modes of GaO_4 and GaO_6 influence the Raman spectrum. In the high-frequency region, the internal modes of GaO_6 and GaO_4 polyhedra are present.

Experimentally, no pressure-induced phase transition upon pressure up to 60 GPa has been observed in the nano-garnets, as expected. However, several *ab initio* calculated IR and silent modes decrease with increasing pressure, thus suggesting a pressure-induced instability at pressure beyond 120 GPa. Indeed, as pointed out above the pressure induce a mechanical instability at 87 GPa. These results for LuGG agree with other theoretical studies of the mechanical and dynamical stability, such as those for the YGG that becomes mechanically unstable at 84 GPa and dynamically unstable at 111 GPa.

Acknowledgements

This work has been supported by Ministerio de Economía y Competitividad of Spain (MINECO) under the National Program of Materials (MAT2013-46649-C4-2/3/4-P) and the Consolider-Ingenio 2010 Program (MALTA CSD2007-0045) and by the EU-FEDER funds. V. Monteseguro, V. Lavín, and V. Venkatramu are also grateful to MINECO from Spain and Department of Science and Technology of India for financial support within the Indo-Spanish Joint Programme of Cooperation in Science and Technology (DST-INT-Spain-P-38-11/PRI-PIBIN-2011-1153). V. Monteseguro wishes to thank MICINN for the FPI grant (BES-2011-044596). F.J. Manjón acknowledges financial support from Generalitat Valenciana through project GVA-ACOMP-2013-012. V. Venkatramu is grateful to DAE-BRNS, Government of India, for the award of DAE Research Award for Young Scientist (No. 2010/20/34/5/BRNS/2223).

Notes and references

[a] Departamento de Física, and MALTA Consolider Team, Universidad de La Laguna. 38200 San Cristóbal de La Laguna, Santa Cruz de Tenerife, Spain.

[b] Instituto de Materiales y Nanotecnología. Universidad de La Laguna. 38200 San Cristóbal de La Laguna, Santa Cruz de Tenerife, Spain.

[c] Instituto de Diseño para la Fabricación y Producción Automatizada, MALTA Consolider Team, Universitat Politècnica de València, Cno. de Vera s/n, 46022 Valencia, Spain

[d] Departamento de Física, Universidad Distrital "Fco. José de Caldas", Bogotá, Colombia

[e] CINVESTAV, Departamento de Nanociencia y Nanotecnología (Zacatenco, México D.F.), Unidad de Querétaro, Querétaro, México

[f] Department of Physics, Yogi Vemana University, 516 003 Kadapa, India.

[g] Department of Physics, Sri Venkateswara University, 517 502 Tirupati, India

[h] Institut of Advances Studies in Atomic, Molecular and Photonics. Universidad de La Laguna. 38200 San Cristóbal de La Laguna, Santa Cruz de Tenerife, Spain.

Fig.1 Unit cell of the $Lu_3Ga_5O_{12}$ garnet structure. The LuO_8 dodecahedron (green), GaO_6 octahedron (blue) and GaO_4 tetrahedron

(pink) polyhedra are highlighted. Green spheres represent the Lu atoms, blue spheres correspond to the Ga atoms, and the small red spheres to the O.

Fig. 2 Evolution of the interatomic distances as a function of the pressure of the $Lu_3Ga_5O_{12}$ garnet. Ga_{tet} stands for Ga atoms with tetrahedral coordination, Ga_{oct} stands for Ga atoms in octahedral coordination. Lu-O1 and Lu-O2 are the smallest and largest Lu-O distances in the distorted LuO_8 dodecahedra.

Fig. 3 Pressure evolution of the elastic constants from 0 to 90 GPa. The red, black, and blue lines correspond to C_{44}, C_{12}, and C_{11}, respectively.

Fig. 4 Pressure evolution of left hand side (M_1, M_2, and M_3) of the generalized Born stability criteria from 0 to 90 GPa.

Fig. 5 Pressure evolution of the bulk modulus (B), shear modulus (G), and Young modulus (E).

Fig. 6 Experimental Raman spectrum of the $Lu_3Ga_5O_{12}$ nano-garnet at ambient conditions. Bottom vertical ticks indicate the *ab initio* frequencies of the Raman active modes.

Fig. 7 Partial and total phonon density of states of the $Lu_3Ga_5O_{12}$ garnet. The total phonon density is the black curve.

Fig. 8 Experimental Raman spectra of the $Lu_3Ga_5O_{12}$ nano-garnet at a function of pressures from 0 up to 60 GPa.

Fig. 9 Theoretical and experimental pressure dependence of the A_{1g}, T_{2g} and E_g Raman modes of the $Lu_3Ga_5O_{12}$ garnet. Lines represent the *ab initio* calculated frequencies and empty squares represent the experimentally observed frequencies. The colours, red and black, in the modes T_{2g} are only used as a guideline for eyes.

Fig. 10 Calculated pressure evolution of the 17 T_{1u} infrared modes of $Lu_3Ga_5O_{12}$.

Fig. 11 Theoretical pressure dependence of the first T_{2u}, T_{1g}, A_{2g} and A_{2u} silent modes of the $Lu_3Ga_5O_{12}$ garnet.

Table I Structural parameters of $Lu_3Ga_5O_{12}$ (LuGG): lattice parameter (a), volume (V_0), bulk modulus (B_0) and bulk modulus derivative (B_0'), and the atomic positions at ambient conditions.

Table II Nearest-neighbor cation-anion distances in $Lu_3Ga_5O_{12}$ crystal at selected pressures.

TABLE III Generalized elastic constants, C_{ij}, bulk modulus, B, isotropic shear modulus, G, Young's modulus, E, Poisson's ratio, γ, Zener anisotropy ratio, A, and B/G ratio $Lu_3Ga_5O_{12}$ garnet structure at zero pressure.

TABLE IV Theoretical (bulk garnet) and experimental (nano-garnet) frequencies, pressure coefficients, and Grüneisen parameters for the Raman-active modes of $Lu_3Ga_5O_{12}$ up to 89 and 60 GPa, respectively. The pressure dependence of both experimental and theoretical frequencies has been fitted with a second order polynomial: $\omega = \omega_o + (\partial\omega/\partial P)\,P + (\partial^2\omega/\partial P^2)\,P^2$.

Table V Theoretical frequencies, pressure coefficients and Grüneisen parameters for the infrared-active modes of bulk $Lu_3Ga_5O_{12}$. The pressure dependence of theoretical frequencies has been fitted with a second order polynomial: $\omega = \omega_o + (\partial\omega/\partial P)\,P + (\partial^2\omega/\partial P^2)\,P^2$.

1 S. F. León-Luis, J. E. Muñoz-Santiuste, V. Lavín, and U. R. Rodríguez-Mendoza, *Opt. Express,* 2012, 20, 10393.

2 V. Venkatramu, M. Giarola, G. Mariotto, S. Polizzi, C. K. Jayasankar, F. Piccinelli, M. Bettinelli, and A. Speghini, *Nanotechnology,* 2010, 21, 175703.

3 D. Jaque, and F. Vetrone, *Nanoscale*, 2012 4, 4301.

4 A. Speghini, F. Piccinelli, and M. Bettinelli, *Opt. Mater*., 2011, 33, 247.

5 Th. Tröster, *Handbook on the Physics and Chemistry of Rare Earths*, edited by K. A. Gschneidner, Jr., J.-C. G. Bünzli and V. K. Pecharsky, Elsevier Science B.V., 2003, 33, Chap. 217, p. 515.

6 S. Karato, Z. Wang, B. Liu, and K. Fujino, *Earth Planet. Sci. Lett*., 1995, 130, 13.

7 L. Seijo, and Z. Barandiaran, *Phys. Chem. Chem. Phys*., 2014, 16, 3830.

8 V. Venkatramu, S. F. León-Luis, A. D. Lozano-Gorrín, L. Jyothi, P. Babu, U. R. Rodríguez-Mendoza, C. K. Jayasankar, J. E. Muñoz-Santiuste, and V. Lavín, *J. Nanosci. Nanotechnol. Chem*., 2012, 12, 4495.

9 K. Papagelis, G. Kanellis, S. Ves, and G. A. Kourouklis, *Phys. Stat. Sol. (b),* 2002, 233, 134-150.

10 K. Papagelis, G. Kanellis, S. Ves, and G. A. Kourouklis, *Phys. Stat. Sol. (b)*, 2003, 235, 348.

11 V. Monteseguro, P. Rodríguez-Hernández, R. Vilaplana, F. J. Manjón, V. Venkatramu, D. Errandonea, V. Lavín, A. Muñoz, *J. Phys. Chem. C*, 2014, 118, 13177.

12 V. Monteseguro, P. Rodríguez-Hernández, V. Lavín, F. J. Manjón, and A. Muñoz*, J. Appl. Phys*., 2013, 113, 183505.

13 H. Guo, M. Zhang, J. Han, H. Zhang, and N. Song, *Physica B* , 2012, 407, 2262.

14 P. Goel, R. Mittal, N. Choudhury and S. L. Chaplot, *J. Phys.: Condens. Matter* , 2010, 22, 065401.

15 A. Mujica, A. Rubio, A. Muñoz, and R.J. Needs, *Rev. Mod. Phys*., 2003, 75, 863.

16 Y.-N. Xu, and W. Y. Ching, *Phys. Rev. B*, 1999, 59, 10530.

17 P. Hohenberg, and W. Kohn, Phys. Rev. 136, 3864 (1964).

18 P. E. Blöchl, *Phys. Rev. B*, 1994, 50, 17953; G. Kresse and D. Joubert, *Phys. Rev. B*, 1999, 59, 1758.

19 J. P. Perdew, A. Ruzsinszky, G.I. Csonka, O. A. Vydrow, G. E. Scuseria, L. A. Constantin, X. Zhou, and K. Burke, *Phys. Rev. Lett*., 2008, 100, 136406.

20 N. Chetty, A. Muñoz, and R. M. Martin, *Phys. Rev. B*, 1989, 40, 11934.

21 S. Baroni, S. de Gironcoli, A. Dal Corso, and P. Giannozzi, *Rev. Mod. Phys*., 2001, 73, 515562.

22 O. Beckstein, J. E. Klepeis, G. L. W. Hart, and O. Pankratov, *Phys. Rev. B*, 2001, 63, 134112.

23 J. F. Nye, *Physical properties of crystals*. *Their representation by Tensor and Matrices,* Oxford University Press, 1957.

24 K. Parlinsky, Computer code PHONON. See: http:// wolf.ifj.edu.pl/phonon

25 F. Yu, D. Yuan, X. Cheng, X. Duan, X. Wang, L. Kong, L. Wang, and Z. Li, *Mat. Lett*., 2007, 61, 2322.

26 V. Venkatramu, S. F. León-Luis, U. R. Rodríguez-Mendoza, V. Monteseguro, F. J. Manjón, A. D. Lozano-Gorrín, R. Valiente, D. Navarro-Urrios, C. K. Jayasankar, A. Muñoz, and V. Lavín. *J. Mater. Chem*., 2012, 22, 13788.

27 H. K. Mao, J. Xu, and P. M. Bell, J. Geophys. Res. 91, 4673 (1986).

28 D. Errandonea, Y. Meng, M. Somayazulu, and D. Hausermann, *Physica B*, 2005, 355, 116.

29 S. Klotz, J.-C. Chervin, P. Munsch, and G. Le Marchand, *J. Phys. D: Appl. Phys.,* 2009, 42, 075413.

30 F. Euler, and J. A. Bruce, Acta Crystallographica 19, 971 (1965).

31 F. Birch, *Phys. Rev.*, 1947, 71, 809.
32 V. Milman, R. H. Nobes, E. V. Akhmatskaya, B. Winkler, C. J. Pickard, and J. A. White, *Ab Initio Study of the Structure and Compressibility of Garnets, in Properties of Complex Inorganic Solids 2*, edited by A. Meike, A. Gonis, P. E. A. Turchi, and K. Rajan, Kluwer Academic/Plenum, New York, 2000, p. 417.
33 V. Monteseguro et al. (unpublished).
34 A. Kaminska, R. Buczko, W. Paszkowicz, H. Przybylinska, E. Wener-Malento, A. Suchocki, M. Brik, A. Durygin, V. Drozd, and S. Saxena, *Phys. Rev. B.,* 2011, 84, 075483.
35 M. Born, and K. Huang, *Dynamical Theory of Crystal Lattices*, Oxford University Press, 1954.
36 J. Wang, S. Yip, S. Phillpot, and D. Wolf, *Phys. Rev. Lett.*, 1993, 71, 4182.
37 B. B. Karki, G. J. Ackland, and J. Crain, *J. Phys.: Condens. Matter.*, 1997, 9, 8579.
38 H. Hua, S. Mirov, and Y. K. Vohra, *Phys. Rev. B*, 1996, 54, 6200.
39 S. F. Pugh, *Philos. Mag.*, 1954, 45, 823.
40 J. Arvanitidis, K. Papagelis, D. Christofilos, H. Kimura, G. A. Kourouklis, and S. Ves, *Phys. Stat. Sol. (b)*, 2004, 241, 3149.
41 J. P. Hurrel, S. P. S. Porto, I. F. Chang, S. S. Mitra, and R. P. Bauman, *Phys. Rev.*, 1968, 173, 851.
42 R. K. Moore, W. B. White, and T. V. Long, *Am. Miner.*, 1971, 56, 54.